Theory of Beam Scanning for Slot Array Antenna Excited by Slow Wave

Arun K. Bhattacharyya, Fellow, IEEE

Lockheed Martin Space Systems, 12257 S. Wadsworth Blvd., Littleton, CO-80125, USA
E-mail: arun.k.bhattacharyya@lmco.com

Abstract

The operating principle of a very special type of slot array antennas excited by a slow-wave mode is presented. The arrays exhibit beam-scanning capability with mechanical rotation about the aperture–normal axis. The relation between the rotation angle and the scan angle is deduced. Numerical results for beam scanning are shown, and other performance characteristics including frequency scan, bandwidth, and polarization of the antennas are presented. Important differences of the characteristic features from that of a conventional array are discussed.

Keywords: Antenna theory; slot array; mechanical scan; slow wave; array antenna

1. Introduction

Typical slot array antennas are fixed beam antennas [1–5]. Although an end-fed waveguide slot array exhibits frequency-scan characteristics, at a given frequency, the beam peak occurs at a fixed look angle. An electronically scanned slot array may be realized by constructing multiple-slot subarrays and exiting each subarray with a power source and a phase shifter as in the case of a conventional phased-array antenna.

A very special type of mechanically scanned slot array is developed by Milroy et al. [6]. A conceptual sketch (exploded view) of an array[1] is shown in Figure 1a. In this type of array, the slots are excited by a slow wave that propagates between the slot plate (plate containing the slots) and the ground plane. Such a slow wave is typically generated by a linear array of waveguides located at one edge, as depicted in Figure 1a. The other edge is typically match terminated. A dielectric layer (as in Figure 1a) or a corrugated ground plane lowers the phase velocity; hence, a slow-wave mode is realized. The waveguide array is attached to the ground plane, and the slot plate is kept free to allow axial rotation about the array–normal axis (z-axis). Nominally, the array creates a beam at a given direction that may be set to the boresight by properly selecting the physical parameters. However, if the slot plate or the ground plane rotates about the z-axis, then the beam scans along a contour on the azimuth-elevation plane. The contour is close to the H-plane trace of the antenna. The scan angle increases with the rotation angle. Thus, by mechanically rotating the slot plate (or the ground plane), one can scan the beam along a contour. For two-dimensional beam scanning, both the slot plate and the ground plane structure should rotate together in addition to a relative rotation between them. This particular antenna configuration does not require any phase shifter, which is very attractive for many applications. To the author's knowledge, nothing is available in the open literature explaining the principle of operation of the array. The purpose of this paper is to present a comprehensive first-order theory that explains the scanning mechanism of the array. An analytical expression of the scan angle as a function of angular rotation, slot spacing, and other physical parameters is obtained. Numerical results demonstrating the beam-scanning capability are shown. The copolarization and cross-polarization of the far-field radiation are analyzed. A shift in the beam position due to the frequency shift is analyzed, and the bandwidth limitation caused by the beam shift is presented. Enhancement of the scan capability to the entire half space and the associated shortcomings are discussed, and the necessary structural modification for performance improvement is suggested. Important differences of

[1] In [6], continuous slots were used, which may be considered as a special case of the general configuration considered here.

Digital Object Identifier 10.1109/MAP.2015.2414532
Date of publication: 17 April 2015

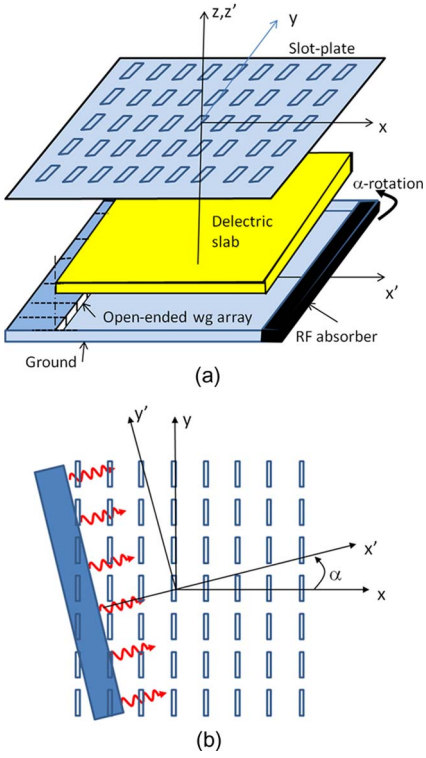

Figure 1. (a) Exploded view of a slot array. The open-ended waveguides produce a slow wave through a dielectric substrate. (b) Coordinate systems for the analytical development. The slow parallel-plate mode (PPM) propagates along the x'-axis.

the scan properties of the array from that of a conventional phased array are discussed.

2. Theory

For simplicity, we assume that the space between the slot plate and the ground plane is filled with a dielectric substrate (see Figure 1a) to support a slow-wave Parallel Plate Mode (PPM). A linear array of waveguides at one edge excites the PPM. The radiating slots are placed in a rectangular grid with cell size $a \times b$. For a boresight beam, the slots must have uniform phase distribution. Typically, for the boresight beam, the slots are oriented perpendicular to the PPM's propagation direction. The uniform phase distribution can be accomplished by placing the slots at λ_g apart in the x-direction λ_g, where λ_g is the wavelength of the PPM. Therefore, to avoid grating lobes near the boresight region, the free-space wavelength must be greater than that of the PPM. We will show analytically that if the slot plate has an angular rotation relative to the ground plane, then the beam mostly scans on a curved surface near the x–z plane (H-plane).

Figure 1b is the top view of the structure. For a general formulation, we assume that the PPM propagates at an angle α with respect to the x-axis. We define a new coordinate system $x'y'z'$ (with $z = z'$) with x' as the wave propagation direction; thus, α is the angle between the x- and x'-axes. Assuming the lowest order transverse magnetic PPM that propagates between the slot plate and the ground plane, the z-component of the electric field can be expressed as

$$E_z(x', y') = E_0 \exp(-j\beta x'). \tag{1}$$

Here, β is the propagation constant of the PPM. Using coordinate transformation from the $x'y'z'$ system to the xyz system, we write (1) as

$$E_z(x, y) = E_0 \exp[-j\beta(x\cos\alpha + y\sin\alpha)]. \tag{2}$$

The equivalent magnetic current on a slot is proportional to the electric field underneath the slot [1]. Accordingly, the magnetic current distribution on the slot at $x = ma$ and $y = nb$ should be

$$M_{ymn}(x, y) = M_y(m, n) f_{slot}(x - ma, y - nb) \tag{3a}$$

with

$$M_y(m, n) = \sigma E_0 \exp[-j\beta(ma\cos\alpha + nb\sin\alpha)]. \tag{3b}$$

In (3b), σ is the coupling coefficient that relates the electric field underneath the slot to the induced magnetic current amplitude on the slot. The field distribution function on the slot is f_{slot}. The equivalent magnetic current will radiate θ- and ϕ-components of the electric field. The total far-field intensity radiated by the slots is obtained as

$$\vec{E}(\theta, \phi) = A\tilde{f}_{slot}(\theta, \phi)(\hat{\theta}\cos\phi - \hat{\phi}\cos\theta\sin\phi) \times \sum_{m,n} M_y(m, n) \exp[jk\sin\theta(ma\cos\phi + nb\sin\phi)] \tag{4}$$

where A is independent of θ and ϕ, k is the wave number in free space, and $\hat{\theta}$ and $\hat{\phi}$ are the unit vectors. The tilda ($\sim$) sign represents Fourier transform. Substituting $M_y(m, n)$ from (3a) and (3b) in (4), we get the far-field vector as

$$\vec{E}(\theta, \phi) = B\sum_{m,n} \exp[jk\sin\theta(ma\cos\phi + nb\sin\phi) - j\beta(ma\cos\alpha + nb\sin\alpha)] \times (\hat{\theta}\cos\phi - \hat{\phi}\cos\theta\sin\phi)\tilde{f}(\theta, \phi) \tag{5}$$

with $B = \sigma E_0 A$. With respect to the principal polarization along x, the copolar and cross-polar fields, using Ludwig's third definition [7], become

$$E_{copol}(\theta, \phi) = B\sum_{m,n} \exp[jk\sin\theta(ma\cos\phi + nb\sin\phi) - j\beta(ma\cos\alpha + nb\sin\alpha)] \times (\cos^2\phi + \cos\theta\sin^2\phi)\tilde{f}(\theta, \phi) \tag{6a}$$

$$E_{cross}(\theta, \phi) = B\sum_{m,n} \exp[jk\sin\theta(ma\cos\phi + nb\sin\phi) - j\beta(ma\cos\alpha + nb\sin\alpha)] \times (1 - \cos\theta)\cos\phi\sin\phi\tilde{f}(\theta, \phi). \tag{6b}$$

Notice that in (6a), the terms under the summation sign add coherently if the following two conditions are simultaneously satisfied (condition for peak intensity):

$$\begin{aligned} a[k\sin\theta\cos\phi - \beta\cos\alpha] &= 2p\pi \\ b[k\sin\theta\sin\phi - \beta\sin\alpha] &= 2q\pi \end{aligned} \tag{7}$$

where p and q are integers. The equations in (7) indicate that by changing α, one can move the beam peak location. That is, by rotating the slot plate with respect to the ground plane (or *vice versa*), one can scan the beam. This is the basic principle of beam scanning of the array under consideration. Setting different values of p and q in (7), one can solve for θ and ϕ for main-lobe and grating-lobe locations. For the main beam at boresight ($\theta = 0$ and $\phi = 0$) corresponding to a frequency f_0 (the design frequency, which is typically the center frequency of a band), we choose $\alpha = 0$. This condition yields

$$a = -2p\pi/\beta_0. \tag{8}$$

In (8), β_0 is the value of β corresponding to the frequency f_0. To minimize the number of grating lobes in the visible region, one prefers a small value of a. To comply, p can be set to negative unity (note that p cannot be zero). Thus, to determine the main beam-peak location, we set $p = -1$ and $q = 0$ in (7). We get

$$\begin{aligned} k\sin\theta\cos\phi &= \beta\cos\alpha - 2\pi/a \\ k\sin\theta\sin\phi &= \beta\sin\alpha. \end{aligned} \tag{9}$$

We now square both sides of the above equations and add together, yielding

$$k^2\sin^2\theta = [\beta\cos\alpha - 2\pi/a]^2 + (\beta\sin\alpha)^2. \tag{10}$$

Using $p = -1$ in (8), one obtains $\beta_0 = 2\pi/a = 2\pi\sqrt{\varepsilon_r}/\lambda_0$, where λ_g is the free-space wavelength at the center frequency f_0, and ε_r is the dielectric constant of the layer between the ground plane and the slot plane. We also use the relation $\beta = k\sqrt{\varepsilon_r} = 2\pi\sqrt{\varepsilon_r}/\lambda$, where λ is the free-space wavelength at the operating frequency. Upon simplification and using above expressions for β and β_0 in (10), we obtain the solution for θ as

$$\theta_{peak} = \sin^{-1}\sqrt{\left(\frac{\lambda_0}{a}\right)^2 + \left(\frac{\lambda}{a}\right)^2 - 2\left(\frac{\lambda\lambda_0}{a^2}\right)\cos\alpha}. \tag{11}$$

Now, eliminating $\sin\theta$ from the equations of (9), we get

$$\tan\phi = \frac{\beta\sin\alpha}{(\beta\cos\alpha - 2\pi/a)}. \tag{12}$$

Substituting the expression for β, we obtain the solution for ϕ as

$$\phi_{peak} = \tan^{-1}\left[\frac{\left(\frac{\lambda_0}{a}\right)\sin\alpha}{\left\{\left(\frac{\lambda_0}{a}\right)\cos\alpha - \lambda/a\right\}}\right]. \tag{13}$$

At the center frequency, the expressions for θ_{peak} and ϕ_{peak} simplify to

$$\begin{aligned} \theta_{peak} &= \sin^{-1}\left[2\left(\frac{\lambda_0}{a}\right)\cos\left(\frac{\alpha}{2}\right)\right] \\ \phi_{peak} &= \frac{(\pi+\alpha)}{2}. \end{aligned} \tag{14}$$

It is worth mentioning that the above expressions for θ_{peak} and ϕ_{peak} assume xyz as the reference coordinate system. For $x'y'z'$ as the reference coordinate system (that is, with respect to the ground plane reference), the value of ϕ_{peak} should be reduced by α, whereas the value of θ_{peak} remains unchanged. Equations (11) and (13) indicate that for given values of a and α, the beam location shifts with frequency as in the case of a typical phased array [8]. Consequently, the gain of the array at a desired location changes with frequency. Accordingly, we define the "instantaneous bandwidth" of the array as the frequency range for which the gain loss lies within 3 dB of the peak gain. The instantaneous bandwidth of the array is given by (see the Appendix)

$$\frac{\Delta f}{f_0} = \frac{0.884}{N_x}. \tag{15}$$

In (15), N_x is the number of slots along x, and Δf is the 3-dB bandwidth. Interestingly, the bandwidth is independent of the number of slots along y, the element spacing, and the scan angle unlike a regular phased-array antenna [8]. Therefore, to attain the maximum possible bandwidth for given aperture dimensions, the value of N_x should be small, which can be accomplished by maximizing the element spacing a along x. The maximum value of a, however, should not exceed λ_0 (in fact, a should be lower than λ_0 because for $a = \lambda_0$, at least one grating lobe exists at the grazing angle even if b is kept sufficiently small) in order to minimize the power loss in the grating lobes.

The scan characteristic can also be graphically understood through a circle diagram [8]. Equation (7) represents an infinite set of circles of radii β (call β-circles) on the $k_x - k_y$ plane, where $k_x = k\sin\theta\cos\phi$, and $k_y = k\sin\theta\sin\phi$. The center of "$(p,q)\beta$-circle" lies on the coordinate point $(2\pi p/a, 2\pi q/b)$, where p and q are integers (see Figure 2). In the visible space, $\sqrt{k_x^2 + k_y^2}$ should be less than k; thus, the area inside the red circle represents the visible space. The arcs of the β-circles inside the visible space represent the beam-peak contours. In Figure 2, multiple such arcs exist, but only the arc of the solid β-circle (the arc BOA in Figure 2) represents the contour of the main lobe peak. This is primarily due to the initial setting of the array (note that with α set to zero, the beam peak occurs at boresight, which is only satisfied by the solid β-circle). Some of the other arcs may represent grating lobe contours. For a given rotation angle α, the locations of the main beam and the grating lobes can be determined from the circle diagram. For instance, point P represents the main beam location for the rotation angle α because the line MP makes an angle α with the k_x-axis. Following the

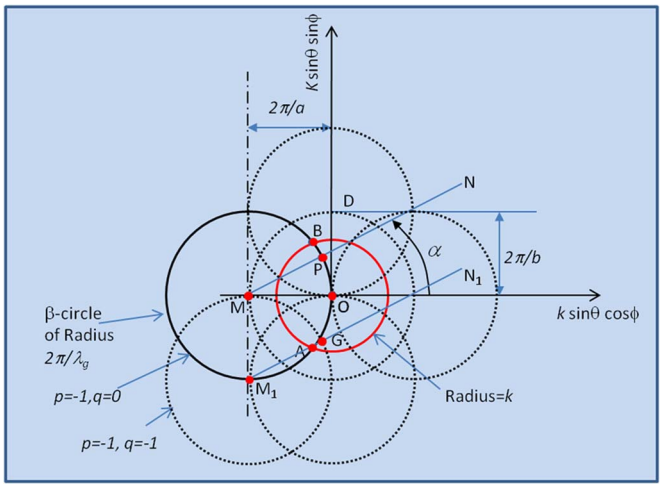

Figure 2. Circle diagram for the slot array. The cell size of the array is $a \times b$. Point P represents the main lobe location with respect to the rotation angle α. Point G represents the grating lobe location for the same rotation angle α. (Note that the lines MN and M_1N_1 are parallel.)

same argument, point G represents the grating lobe because the line M_1G makes an angle α with the k_x-axis.

The circle diagram can be employed to determine the element spacing for an array. For instance, if the main beam needs to be at boresight for $\alpha = 0$, then the solid β-circle must pass through the origin of the $k_x - k_y$ plane. This happens if $a = \lambda_g$. If $a < \lambda_g$, then the main beam will not scan through the boresight. Moreover, for continuous slots along y, only one row of β-circles exists as b can be assumed as zero. As a result, points such as G will not exit, indicating nonexistence of grating lobes. If, however, a becomes larger than λ_g, then grating lobes may exist.

3. Numerical Results and Discussions

In order to demonstrate the beam-scanning capability of the array under consideration, we compute the copolar patterns for various values of the rotation angle α. We use (6a) and consider the propagation constant β_0 of the PPM as $2k_0$. Such a slow PPM can be generated either by using a high dielectric material of dielectric constant 4 between the plates or by using corrugated bottom layer that supports a slow-wave mode [9]. Using $\beta_0 = 2k_0$ in (8) and with $p = -1$, the slot spacing a becomes $\lambda_0/2$ (λ_0 = free space wavelength). We also set $b = \lambda_0/2$ to avoid grating lobes. Figure 3 shows the normalized pattern cuts (with respect to the peak intensity) of an array with 20 × 20 slots. The pattern cuts are computed on the $\phi = \phi_{peak}$ planes to show the movement of the beam peak. The slot radiation pattern was ignored [which is a multiplication factor in (6a)] for the plot. Notice that the beam location moves from the boresight as α increases. For maximum scan angle ($\theta_{peak} = 90°$), the value of α should be equal to $2\sin^{-1}(k_0/2\beta_0)$. For the present case, the corresponding value of α is 28.96°. Notice that, for this α, the

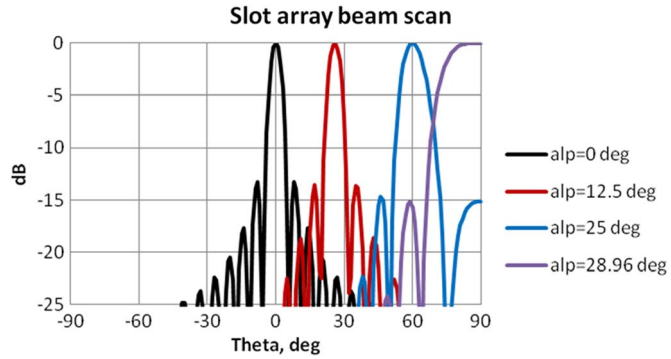

Figure 3. Beam scanning with mechanical rotation (alp = α = rotation angle). The parameters are: $a = b = \lambda_0/2$, dielectric constant = 4.0, $N_x = N_y = 20$.

beam peak occurs at $\theta = 90°$ with increased beamwidth, which is expected from a scanned beam [8].

Figure 4a and b is the copolar and cross-polar contours of a scanned beam on the $\theta_x - \theta_y$ plane, where $\theta_x = \theta\cos_\phi$, and $\theta_y = \theta\sin_\phi$. For this case, we set $\beta_0/k_0 = 1.5$, $a = b = 0.67\lambda_0$, and $\alpha = 25°$. The beam peak occurs at $\theta = 40.49°$ and $\phi = 102.5°$. Notice that a grating lobe is observed near $\theta = 61.3°$ and $\phi = 260.8°$ (near the θ_y-axis). This grating lobe is due to the larger slot spacing along y. No grating lobe

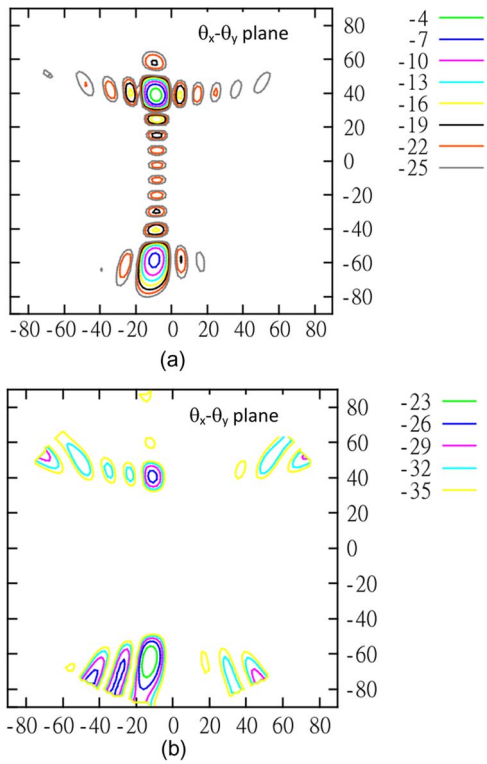

Figure 4. Copolarization and cross-polarization contours for a scanned beam with $\alpha = 25°$, $\beta = 1.5k_0$, and $a = b = 0.667\ \lambda_0$. Horizontal axis: $\theta\cos\phi$; vertical axis: $\theta\sin\phi$ (both in degrees). The main beam peak occurs at $\theta = 40.49°$ and $\phi = 102.5°$. The grating lobe is at $\theta = 61.3°$ and $\theta = 260.8°$. (a) Copolarization. (b) Cross-polarization.

occurs near the θ_x-axis because the grating lobes along this axial region exist beyond the visible space. If, however, the slot spacing along x exceeds one wavelength, grating lobes will occur near the θ_x-axis. The cross-polarization level in Figure 4b is below 23 dB near the main beam peak. The cross-polarization is low near the principal planes due to the symmetry of the source fields. It is worth mentioning that the value of b has no role in determining the beam peak location. Its value is solely decided by the grating lobe consideration.

Figure 5 shows the loci of the main beam peaks on the $\theta_x - \theta_y$ plane with β_0/k_0 (denoted by F in the inset of Figure 5) as a parameter. A locus essentially corresponds to the arc BOA in Figure 2 mapped onto the $\theta_x - \theta_y$ plane from the $k_x - k_y$ plane. From (14), the locus of the beam peak is deduced as $\sin\theta_{peak} = -(2\beta_0/k_0)\cos\phi_{peak}$. Since the left-hand side is positive, the equation satisfies if the locus lies on the second and third quadrants of the $\theta_x - \theta_y$ plane, as depicted in Figure 5. Notice that the beam loci are very close to the $\phi = 90^\circ$ line with some deviation with the scan angle. The deviation decreases with increasing β_0/k_0. This is consistent with (14) because for a given θ_{peak}, the value of α should be smaller for a larger β_0/k_0; hence, ϕ_{peak} becomes smaller.

Equations (11) and (13) indicate that for a given α, the beam peak location moves with frequency because θ_{peak} and ϕ_{peak} are functions of the wavelength λ. To study this "frequency-scan" behavior, we plot the beam contours at three representative frequencies covering 5% bandwidth in Figure 6. We use 21 × 21 slots and the rotation angle α as 25°. Interestingly, the frequency-scan occurs almost parallel to the horizontal axis (see (18) in the Appendix). This is contrary to a regular phased array where the "frequency-scan" occurs on $\phi =$ constant plane. The gain rolloff for the beams associated with the upper and lower end frequencies at the desired location (corresponding to the beam peak location at midfrequency) is about 4 dB. This implies that the array

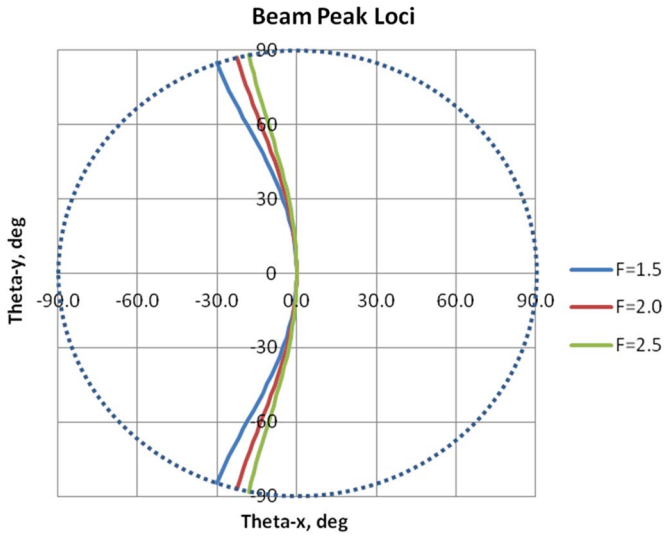

Figure 5. Loci of beam peaks for three different values of $F(=\beta_0/k_0 = \varepsilon_r^{1/2})$. The plot is on the $\theta_x - \theta_y$ plane, where $\theta_x = \theta\cos\phi$, and $\theta_y = \theta\sin\phi$.

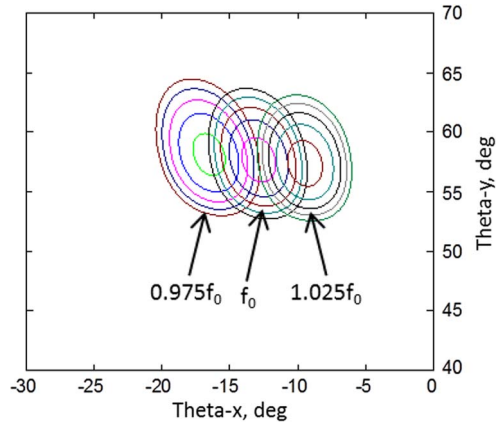

Figure 6. Copolarization contours on the $\theta_x - \theta_y$ plane (showing beam deviation with frequency) at three frequencies (0.975 f_0, f_0 and 1.025 f_0) with $\alpha = 25^\circ$, $N_x = N_y = 21$, $a = b = 0.5\lambda_0$, and $\beta/k = 2$. Notice that the beams deviate almost parallel to the θ_x-axis. The elliptical contours are 1 dB apart.

does not satisfy a 5% bandwidth requirement with respect to 3-dB gain loss. In fact, the bandwidth of this array should be about 4.2% as per (15). To have 5% bandwidth, the number of slots along the x-direction should not exceed 17 ($N_x < 17$).

In Figure 7, we have plotted the beam peak loci by varying the rotation angle α at three different frequencies. The small circle marks on the curves are associated with different values of α starting from zero to 28° with 1° interval (a total of 29 marks on each curve). Notice that the "frequency-scan" increases with α; that is, the more the scan angle, the more is the beam deviation with frequency. However, the beamwidth increases with the scan angle in such a way that it compensates the additional gain rolloff, keeping the bandwidth unchanged. An analytical proof of this interesting behavior is shown in the Appendix. In a regular phased array, however, the bandwidth decreases with the scan angle.

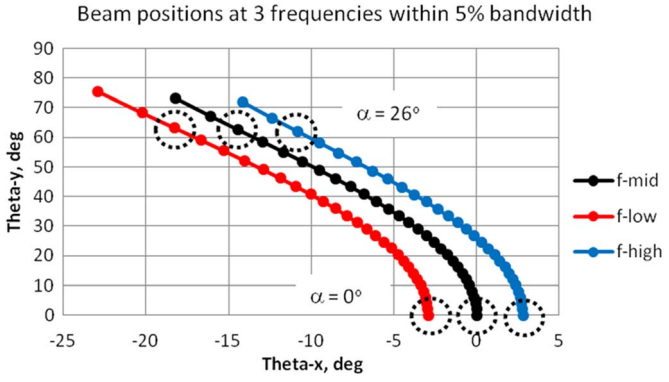

Figure 7. Beam-peak loci at three frequencies (f − mid = f_0, f − low = 0.975 f_0, and f − high = 1.025 f_0). Each marker on a curve corresponds to a rotation angle α (that varies from 0° to 28°). Note that the beam separation increases with α (hence with the scan angle). Moreover, for each α, the beam scans with frequency irrespective of its value.

As mentioned before, to enhance the scanning capability to the entire half space, both the plates must be rotated together in addition to a relative rotation between the plates. Consequently, the principal polarization rotates with the slot plate, which is not a desirable feature for practical applications. In particular, the polarization rotation causes a polarization mismatch with the receiving antenna (assuming the antenna under consideration is transmitting). One way to circumvent the above problem is to convert the linear polarization to a circular polarization because the latter does not have any preferred polarization orientation. This can be accomplished by incorporating a meander-line screen polarizer [10] that should be attached to the slot plate. If, however, the linear polarization has to be maintained, then the array may be loaded with two meander-line screen polarizers. By adjusting the relative orientations, a linear polarization with a desired polarization direction can be achieved [11]. The first polarizer (to be attached with the slot plate) will convert linear to circular polarization. The second polarizer should be kept at a fixed orientation (depending on the desired orientation of the copolarization vector). The second polarizer converts circular lo linear polarization with the desired polarization angle. This is schematically shown in Figure 8. It is also possible to remove the first polarizer completely. In that case, the slots must be loaded with waveguide sections. By incorporating diagonal strips, one can convert linear to circular polarization. Moreover, the length of the waveguide section can be adjusted to control the coupling between PPM and slot fields, which is necessary to properly design the array.

In order to validate the analytical model presented in this paper, we compare the predicted radiation pattern of a scanned beam with the available measured data [12]. In

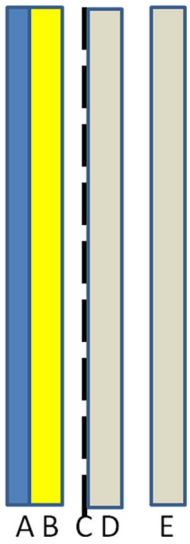

Figure 8. Cross-sectional view of a screen-polarizer loaded array. A = WG array, B = dielectric slab, C = slot plate, D = Polarizer 1, E = Polarizer 2. A and B rotate together, and C and D rotate together. Their rotation angles depend on the beam location. E is kept fixed for a given polarization angle. For circular polarization, E should be removed.

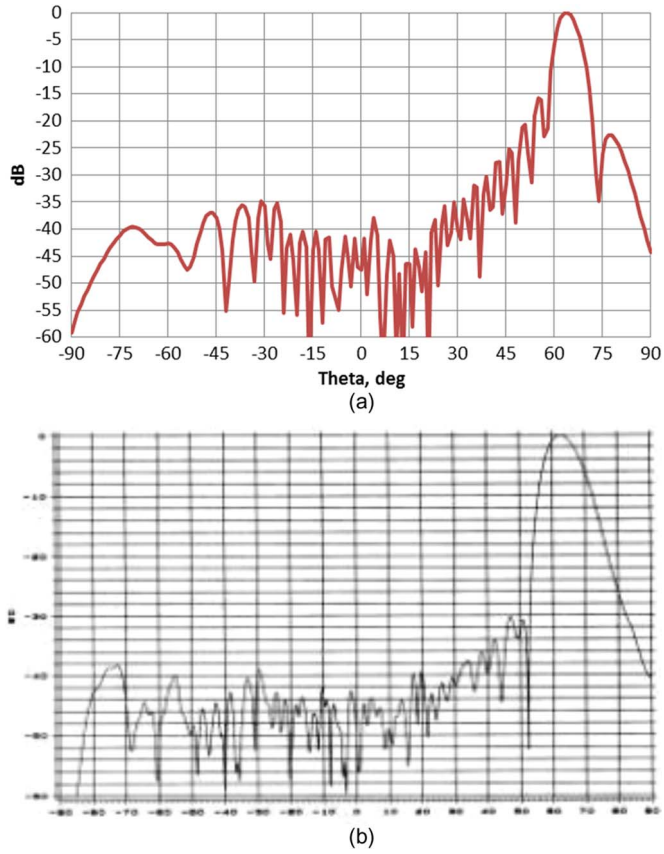

Figure 9. Computed and measured radiation patterns of a 20-inch-diameter array at 12.5 GHz and at 63° scan. For computed data, the dielectric constant was assumed as 3.24° and $\alpha = 28.7°$. (a) Computed. (b) Measured [12, Figure 8].

Figure 9, we present the results of a Ku-band array of 20-in diameter. The scan angle is about 63° off boresight. We assume the dielectric constant of the layer between the slot plane and the ground plane as 3.24. For such a structure, the 63° scan beam can be accomplished with a relative rotation of 28.7°. The agreement between computed and measured patterns is satisfactory. The measured pattern has a wider beamwidth than that of the computed pattern. This is primarily due to the amplitude taper and the phase error due to fabrication tolerance. For the computed pattern, we assume uniform amplitude taper because no taper information is given in [12].

4. Conclusion

In this paper, we have presented a simple mathematical theory that explains the beam scanning caused by the rotation of the slot plate relative to the ground plane. The governing equations leading to a top-level design of such an array are deduced. The analysis reveals the following important characteristic features of the array.

- The scan angle increases with the rotation angle, and the scan occurs almost along the H-plane of the antenna with a minor deviation. The angular

deviation from the H-plane is half the rotation angle.

- For a given rotation angle, the beam scans with frequency. Unlike a conventional phased-array antenna, this "frequency-scan" does not occur on the scan plane. Furthermore, the "frequency-scan" occurs for all scan angles including boresight. In the case of a conventional array, the frequency scan does not occur for a boresight beam, however.

- The instantaneous bandwidth (based on the 3-dB gain loss) is only dependent on the number of slots along the E-plane direction. It is independent of other antenna parameters.

It must be mentioned that although the instantaneous bandwidth is not too large, the array can be used for multiple switchable bands. The beam-peak contour will shift from band to band, however. The overall operating bandwidth could be large because the structure can support a PPM over a wide frequency range. The analysis presented here may be adequate for understanding the basis characteristic features of the antenna, but a detailed analysis requires rigorous computations of coupling coefficients between the slots and the PPM, incorporation of the mutual coupling effects between the slots, and inclusion of the effects of higher order modes in the parallel-plate region.

5. Appendix

To deduce the bandwidth relation in (15), we begin with the copolar array pattern given in (6a). Thus

$$E_{copol}(\theta,\phi) = B\sum_{m,n}\exp[\,jk\sin\theta(ma\cos\phi + nb\sin\phi) - j\beta(ma\cos\alpha + nb\sin\alpha)] \times (\cos^2\phi + \cos\theta\sin^2\phi)\tilde{f}(\theta,\phi). \quad (16)$$

After summing up over m and n, a closed-form expression can be obtained as

$$E_{copol}(\theta,\phi) = \frac{\sin\left\{\frac{N_x ka}{2}(\sin\theta\cos\phi - F\cos\alpha)\right\}\sin\left\{\frac{N_y kb}{2}(\sin\theta\sin\phi - F\sin\alpha)\right\}}{\sin\left\{\frac{ka}{2}(\sin\theta\cos\phi - F\cos\alpha)\right\}\sin\left\{\frac{kb}{2}(\sin\theta\sin\phi - F\sin\alpha)\right\}} \quad (17)$$

In (17), $F = \beta/k$, and N_x and N_y are the number of slots along the x- and y-directions, respectively. We ignored the amplitude factor because, for the bandwidth analysis, only the relative amplitude matters. Moreover, the factor $(\cos^2\phi + \cos\theta\sin^2\phi)\tilde{f}(\theta,\phi)$ is ignored because for a narrow beam, this factor can be treated as a constant within the 3-dB beamwidth. For a beam peak, the value of q in (7) is zero, so that we get

$$\sin\theta\sin\phi - F\sin\alpha = 0. \quad (18)$$

Notice that the above relation is independent of frequency. Therefore, we can say that for a given rotation angle α, the beam peaks at different frequencies lie on the curve represented by (18). Combining (17) and (18), we obtain the array pattern along the beam-peak locus as

$$E_{copol}(\theta,\phi) = \frac{\sin\left\{\frac{N_x ka}{2}(\sin\theta\cos\phi - F\cos\alpha)\right\}}{\sin\left\{\frac{ka}{2}(\sin\theta\cos\phi - F\cos\alpha)\right\}}. \quad (19)$$

At the design frequency (midfrequency of the band), we have

$$ka(\sin\theta\cos\phi - F\cos\alpha) = -2\pi \quad (20)$$

as per (7). The magnitude of E_{copol} should be equal to N_x. At the upper-end frequency of the band, the magnitude of E_{copol} should be 3 dB lower than that at midfrequency. Therefore, we must solve for k' such that

$$\left|\frac{\sin\left\{\frac{N_x k'a}{2}(\sin\theta\cos\phi - F\cos\alpha)\right\}}{\sin\left\{\frac{k'a}{2}(\sin\theta\cos\phi - F\cos\alpha)\right\}}\right| = \frac{N_x}{\sqrt{2}}. \quad (21)$$

For a large N_x (greater than 7), (21) has the following solution in the neighborhood of its peak value:

$$\frac{N_x k'a}{2}(\sin\theta\cos\phi - F\cos\alpha) = -N_x\pi - 1.39. \quad (22)$$

From (20) and (22), we get

$$\frac{k'-k}{k} = \frac{1.39}{\pi N_x}. \quad (23)$$

This yields the fractional bandwidth as

$$\frac{\Delta f}{f_0} = \frac{2\times 1.39}{\pi N_x} = \frac{0.884}{N_x} \quad (24)$$

where f_0 is the midfrequency corresponding to the wave number k. The factor 2 is due to the two sides of the band from the midfrequency.

6. References

[1] R. T. Compton, Jr. and R. E. Collin, "Slot antennas," in *Chapter 14 in Antenna Theory*, Part 1,R. E. Collin andF. J. Zucker eds. New York, NY, USA: McGraw-Hill, 1969.

[2] R. S. Elliott, "The Design of Waveguide-Fed Slot Arrays," in *Antenna Handbook*,Y. T. Lo and S. W. Lee eds. New York, NY, USA: Van Nostrand Rheinhold, 1988.

[3] S. R. Rengarajan and A. G. Derneryd "Application of compound coupling slots in the design of shaped beam antenna patterns," *IEEE Trans. Antennas Propag.*, vol. 41, no. 1, pp. 59–65, Jan. 1993.

[4] K.-S Min et al., "A circularly polarized waveguide narrow-wall slot array using a single layer polarization converter," in *Proc. IEEE Antennas Propag. Soc. Symp. Dig.*, Jul. 1996, pp. 1004–1007.

[5] Q. Yang, X. Zhao, and Y. Zhang, "Composite right/left-handed ridge substrate integrated waveguide slot array antennas," *IEEE Trans. Antennas Propag.*, vol. 62, no. 4, pp. 2311–2315, Apr. 2014.

[6] W. W. Milroy, S. B. Coppedge, and A. C. Lemons, "Variable inclination continuous transverse stub array,"U.S. Patent 6 919 854 B2, Jul. 19, 2005.

[7] A. C. Ludwig, "The definition of cross polarization," *IEEE Trans. Antennas Propag.*, vol. AP-21, no. 1, pp. 116–119, Jan. 1973.

[8] A. K. Bhattacharyya, *Phased Array Antennas- Floquet Analysis, Synthesis, BFNs, and Active Array Systems*. Hoboken, NJ, USA: Wiley, 2006.

[9] A. K. Bhattacharyya, "High-Q resonances due to surface waves and their effects on the performances of corrugated horns," *IEEE Trans. Antennas Propag.*, vol. AP-49, no. 4, pp. 555–566, Apr. 2001.
[10] A. K. Bhattacharyya and T. J. Chwalek, "Analysis of multilayered meander line polarizer," *Int. J. Microw. Millimeter-Wave Comput. Aided Eng.*, vol. 7, no. 6, pp. 442–454, Jul. 1997.
[11] J.-C Zhang, Y.-Z Yin, and J.-P. Ma, "Multifunctional meander line polarizer," *Progr. Electromagn. Res. Lett.*, vol. 6, pp. 55–60, 2009.
[12] W. W. Milroy, "Advanced broadband access applications of the Continuous Transverse Stub (CTS) array," in *Proc. ICEAA*, Torino, Italy, Sep. 2001.

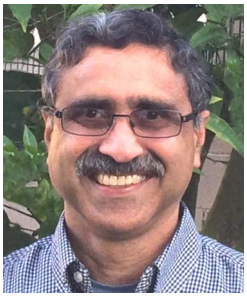

Arun K. Bhatacharyya (M'87–SM'91–F'02) received the B.Eng. degree in electronics and telecommunication engineering from Bengal Engineering College, University of Calcutta, Kolkata, India, in 1980 and the M.Tech. and Ph.D. degrees from the Indian Institute of Technology Kharagpur, Kharagpur, India, in 1982 and 1985, respectively.

From November 1985 to April 1987, he was a Postdoctoral Fellow with the Department of Electrical Engineering, University of Manitoba, Winnipeg, MB, Canada. From May 1987 to October 1987, he was a Senior Antenna Engineer with Til-Tek Limited, Kemptville, ON, Canada. In October 1987, he joined the University of Saskatchewan, Saskatoon, SK, Canada, as an Assistant Professor with the Department of Electrical Engineering and then as an Associate Professor in 1990. In July 1991, he joined Boeing Satellite Systems (formerly Hughes Space and Communications), Los Angeles, CA, USA, as a Senior Staff Engineer, and then promoted to Scientist and Senior Scientist ranks in 1994 and 1998, respectively. He became a Technical Fellow of Boeing in 2002. In September 2003, he joined the Northrop Grumman Space Technology group as a Staff Scientist (senior grade) and became a Distinguished Engineer and Engineering Fellow. He is currently with Lockheed Martin Space System, Littleton, CO, USA. He is the author of "Electromagnetic Fields in Multilayered Structures—Theory and Applications" (Artech House, Norwood, MA, 1994) and "Phased Array Antennas, Floquet Analysis, Synthesis, BFNs and Active Array Systems" (Hoboken, Wiley, 2006). He authored over 95 technical papers and five book chapters and has 16 issued patents. His technical interests include electromagnetics, printed antennas, multilayered structures, active phased arrays, and modeling of microwave components and circuits.

Dr. Bhattacharyya was a recipient of numerous awards, including the 1996 Hughes Technical Excellence Award, the 2002 Boeing Special Invention Award for his invention of high-efficiency horns, the 2003 Boeing Satellite Systems Patent Awards, and the 2005 Tim Hannemann Annual Quality Award, Northrop Grumman Space Technology.